Nitrogenase-mimic iron-containing chalcogels for photochemical reduction of dinitrogen to ammonia

Jian Liu[a,b], Matthew S. Kelley[a,b], Weiqiang Wu[a,b], Abhishek Banerjee[a,b], Alexios P. Douvalis[c], Jinsong Wu[a,b], Yongbo Zhang[a,b], George C. Schatz[a,b,1], and Mercouri G. Kanatzidis[a,b,1]

[a]Department of Chemistry, Northwestern University, Evanston, IL 60208; [b]Argonne-Northwestern Solar Energy Research Center, Northwestern University, Evanston, IL 60208; and [c]Department of Physics, University of Ioannina, 45110 Ioannina, Greece

Contributed by George C. Schatz, April 11, 2016 (sent for review February 25, 2016; reviewed by Kyoung-Shin Choi and Lance C. Seefeldt)

A nitrogenase-inspired biomimetic chalcogel system comprising double-cubane [$Mo_2Fe_6S_8(SPh)_3$] and single-cubane (Fe_4S_4) biomimetic clusters demonstrates photocatalytic N_2 fixation and conversion to NH_3 in ambient temperature and pressure conditions. Replacing the Fe_4S_4 clusters in this system with other inert ions such as Sb^{3+}, Sn^{4+}, Zn^{2+} also gave chalcogels that were photocatalytically active. Finally, molybdenum-free chalcogels containing only Fe_4S_4 clusters are also capable of accomplishing the N_2 fixation reaction with even higher efficiency than their $Mo_2Fe_6S_8(SPh)_3$-containing counterparts. Our results suggest that redox-active iron-sulfide–containing materials can activate the N_2 molecule upon visible light excitation, which can be reduced all of the way to NH_3 using protons and sacrificial electrons in aqueous solution. Evidently, whereas the $Mo_2Fe_6S_8(SPh)_3$ is capable of N_2 fixation, Mo itself is not necessary to carry out this process. The initial binding of N_2 with chalcogels under illumination was observed with in situ diffuse-reflectance Fourier transform infrared spectroscopy (DRIFTS). $^{15}N_2$ isotope experiments confirm that the generated NH_3 derives from N_2. Density functional theory (DFT) electronic structure calculations suggest that the N_2 binding is thermodynamically favorable only with the highly reduced active clusters. The results reported herein contribute to ongoing efforts of mimicking nitrogenase in fixing nitrogen and point to a promising path in developing catalysts for the reduction of N_2 under ambient conditions.

nitrogenase mimics | chalcogel | N_2 fixation | ammonia synthesis | photocatalytic

The reduction of atmospheric nitrogen to ammonia is one of the most essential processes for sustaining life. Currently, roughly half of the fixed nitrogen is supplied biologically by nitrogenase, while nearly the other half is from the industrial Haber–Bosch process, which operates under high temperature (400–500 °C) and high pressure (200–250 bar) in the presence of a metallic iron catalyst (1). Nitrogenase, a two-component protein system comprising a MoFe protein and an associated Fe protein, carries out this "fixation" in nature under ambient temperature and pressure (2–4). N_2 substrate binding and activation take place at the iron–molybdenum–sulfur cofactor (FeMoco), and in some cases, Mo-free iron–sulfur cofactor FeFeco and iron–vanadium–sulfur cofactor FeVco cofactors. Electron transfer during this catalytic process is believed to proceed from a [4Fe:4S] cluster located in the Fe protein to another Fe/S cluster (the P cluster) buried in the MoFe protein and finally to the FeMoco (Fig. 1*A*) (2, 5, 6). Whereas the role of Mo in the reactivity of nitrogenase has been the subject of long debate, iron is now well recognized as the only transition metal essential to all nitrogenases, and recent biochemical and spectroscopic data point to iron as the site of N_2 binding in the FeMoco (7–9). Naturally, understanding and mimicking how the nitrogenase enzyme accomplishes the difficult task of N_2 reduction under ambient conditions is one of the grand challenges in chemistry. To this end, inspired by the molecular structure and function of FeMoco, a number of groups have synthesized transition metal–dinitrogen complexes and examined stoichiometric transformations of their coordinated N_2 into NH_3 and N_2H_4 (9–19). However, the operation of homogeneous transition metal–dinitrogen complexes usually requires organic solvents, strong reducing agents, and often extremely low operation temperatures (5, 10, 12, 14). The prospect of using solar light energy to convert N_2 to ammonia is highly attractive but it represents a great challenge and is a less-investigated line of inquiry. Hamers and co-workers reported that solvated electrons emitted from illuminated diamond can accomplish N_2 reduction (20, 21). Other semiconductor systems such as $Fe_2Ti_2O_7$ (22), Au/Nb–$SrTiO_3$/Ru (23), and $BiOBr_{ov}$ (24) were also reported to perform light-induced N_2 fixation. These systems are not biomimetic and usually exhibit very low conversion efficiency (*SI Appendix*, Table S1).

Our group has recently developed a new class of porous chalcogenide aerogels by the metathesis reaction, dubbed "chalcogels," which can be functionalized with biomimetic functionalities (25–27). These materials can easily incorporate $Mo_2Fe_6S_8(SPh)_3$ or Fe_4S_4 clusters in their structure and have been shown to reduce protons both electrocatalytically and photocatalytically to hydrogen (28, 29). The $Mo_2Fe_6S_8(SPh)_3$ cluster-based chalcogel was recently demonstrated to be capable of photocatalytically reducing N_2 to NH_3 (30). Inspired by the structure and function of the MoFe protein of nitrogenase which contains both iron–molybdenum–sulfur and iron–sulfur clusters (the P cluster), we prepared a chalcogel that also incorporated two types of clusters: the FeMoco-like $Mo_2Fe_6S_8(SPh)_3$ and P-cluster–like Fe_4S_4 linked together with units of $[Sn_2S_6]^{4-}$, in a 3D superstructure (Fig. 1*B*) (2, 4, 30). This chalcogel is dubbed "FeMoS–FeS-SnS." We also prepared two more chalcogels, one with $Mo_2Fe_6S_8(SPh)_3$ clusters and inert metals such as Sb^{3+}, Sn^{4+}, Zn^{2+} (dubbed "FeMoS–M-SnS") and a molybdenum-free one, the Fe_4S_4 chalcogel (FeS–SnS) (31, 32). The purpose of using the

Significance

In nature, nitrogenase fixes nitrogen into biologically usable forms under ambient conditions. Today, half of the world's nitrogen fixation is achieved through the industrial Haber–Bosch process, which operates at elevated temperature and pressure. Here, we present a synthetic nitrogenase mimic in the form of chalcogel composed of molybdenum and iron-containing biomimetic clusters that can accomplish photocatalytic N_2 fixation and conversion to NH_3 at ambient temperature and pressure. Surprisingly, the iron–sulfur chalcogels without molybdenum are observed to have a higher activity toward N_2 reduction. The results reported here will greatly expand the scope of materials design and engineering for the creation of highly active iron-based N_2 reduction catalysts operating in mild conditions.

Author contributions: J.L., M.S.K., G.C.S., and M.G.K. designed research; J.L., M.S.K., W.W., A.B., A.P.D., J.W., and Y.Z. performed research; W.W., A.P.D., J.W., and Y.Z. contributed new reagents/analytic tools; J.L., M.S.K., W.W., A.B., A.P.D., J.W., Y.Z., G.C.S., and M.G.K. analyzed data; and J.L., M.S.K., G.C.S., and M.G.K. wrote the paper.

Reviewers: K.-S.C., University of Wisconsin; and L.C.S., Utah State University.

The authors declare no conflict of interest.

[1]To whom correspondence may be addressed. Email: g-schatz@northwestern.edu or m-Kanatzidis@northwestern.edu.

This article contains supporting information online at www.pnas.org/lookup/suppl/doi:10.1073/pnas.1605512113/-/DCSupplemental.

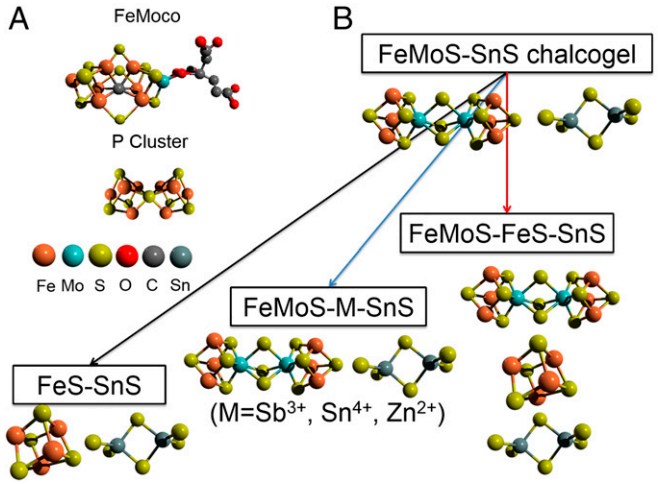

Fig. 1. Nitrogenase-inspired biomimetic chalcogels. (*A*) The two-component proteins of molybdenum nitrogenase: MoFe protein and Fe protein; space filling and stick model structures of the FeMo cofactor and the P cluster. (*B*) The reaction routes leading to the assembly of FeMoS–SnS, FeMoS–FeS–SnS, and FeMoS–M–SnS (M=Sb^{3+}, Sn^{4+}, Zn^{2+}) chalcogel, respectively.

FeMoS–M–SnS chalcogels was to see if placing the FeMoS clusters farther apart in space would have any effect on the catalytic reaction, whereas that of FeS–SnS was to probe the necessity of Mo. These three chalcogels achieve photocatalytic N_2 reduction but more importantly, and to our surprise, the iron-only FeS–SnS chalcogel is in fact not only capable of N_2 reduction but also with higher rate. Diffuse-reflectance Fourier transform infrared spectroscopy (DRIFTS) experiments performed under light illumination show a clear signature of the N_2 binding process and its subsequent reduction. The results reported here show that the photochemical activation of N_2 using visible light is possible with $Mo_2Fe_6S_8(SPh)_3$ as well as Fe_4S_4-based materials at room temperature, ambient pressure, and aqueous conditions. Despite the complex progression multielectron/-proton reactions required, we clearly have an unexpectedly viable and robust process that leads to ammonia. Our results also demonstrate that iron rather than molybdenum is the element necessary for photoreduction of N_2 to NH_3.

Results and Discussion

The relatively facile bottom-up synthesis of chalcogels enables variation of components with easy integration into the structure (25, 26). Aiming at a boost in the photochemical N_2 reduction yield, we devised the construction of a new chalcogel (FeMoS–FeS–SnS) incorporating both $Mo_2Fe_6S_8(SPh)_3$ and Fe_4S_4 clusters as a closer mimic of nitrogenase. To study the role of Mo in the catalytic mechanism, we made two different modifications to the chalcogel. In one we used redox-inert ions instead of Fe_4S_4 clusters to construct FeMoS–M–SnS chalcogels, where M=Sb^{3+}, Sn^{4+}, Zn^{2+}. In the second, we used only Fe_4S_4 clusters for a Mo-free chalcogel. Fig. 2*A* shows schematic illustration of the 3D network. The synthetic reactions to prepare these chalcogels are given in the *SI Appendix*, Table S2.

Typical images of the FeMoS–FeS–SnS chalcogel are shown in Fig. 2*B*. The shiny and flat cleaved surface of the chalcogel indicates excellent gelation status. Scanning electron microscopy (SEM) characterization in Fig. 2*C* reveals the spongy and porous nature of the chalcogel. Transmission electron microscopy (TEM) in Fig. 2*D* further demonstrates the porosity of the chalcogel; selected-area electron diffraction as well as X-ray diffraction patterns (*SI Appendix*, Fig. S1*A*) confirm the amorphous character. The chalcogel can turn into a highly porous aerogel after supercritical drying with CO_2 whose surface area is high as assessed with nitrogen adsorption measurements (Fig. 2*E*). Fig. 2*F* shows a typical cyclic voltammetry (CV) curve obtained from FeMoS–FeS–SnS chalcogel immobilized on the surface of the glassy carbon electrode. Two distinct reduction waves are observed, occurring at approximately –870 and –1,250 mV, and indicate that $Mo_2Fe_6S_8(SPh)_3$ and Fe_4S_4 clusters in the chalcogel network are redox active. The adsorption–desorption isotherms show a type IV adsorption branch and gave a 150-m^2/g surface area. The Mössbauer spectrum recorded at 77 K shows the presence of both Fe_4S_4 and $Mo_2Fe_6S_8(SPh)_3$ clusters into the chalcogel (Fig. 2*G*). This spectrum is composed of a main central quadrupole split part, which was fit using a combination of two pairs of components of equal areas. Elemental analysis (*SI Appendix*, Fig. S1*C*) of FeMoS–FeS–SnS aerogel shows the presence of all of the expected elements. The presence of counter cations Ph_4P^+ and Na^+ indicates the chalcogel network is overall negatively charged. The presence of clusters in chalcogels was also assessed with thiol extrusion experiments as described previously (*SI Appendix*, Fig. S1*D*) (27, 29, 31). The chalcogels are black and have very strong and broad optical absorption in the visible range (27, 28, 30).

The simplified N_2 reduction equation is depicted in Fig. 3*A* (30). In a typical experiment, slices of chalcogels were put into a sealable vial containing 5 mM NaAc and 50 mM PyrH aqueous solution (*SI Appendix*, Table S3, entry 1). The expected NH_3 will protonate to NH_4^+ in the slightly acidic reaction environment (pH = 4). Fig. 3*B* shows the ^{1}H NMR of NH_4^+ samples obtained in a typical photocatalytic reaction (see the full NMR spectrum in *SI Appendix*, Fig. S2 and the calibration curve of $^{14}NH_4Cl$ in *SI Appendix*, Fig. S3). Fig. 3*C* shows NH_4^+ production from photochemical reduction of N_2 on FeMoS–FeS–SnS, FeMoS–M–SnS, and FeS–SnS chalcogels, respectively (see *SI Appendix*, Figs. S4 and S5 for

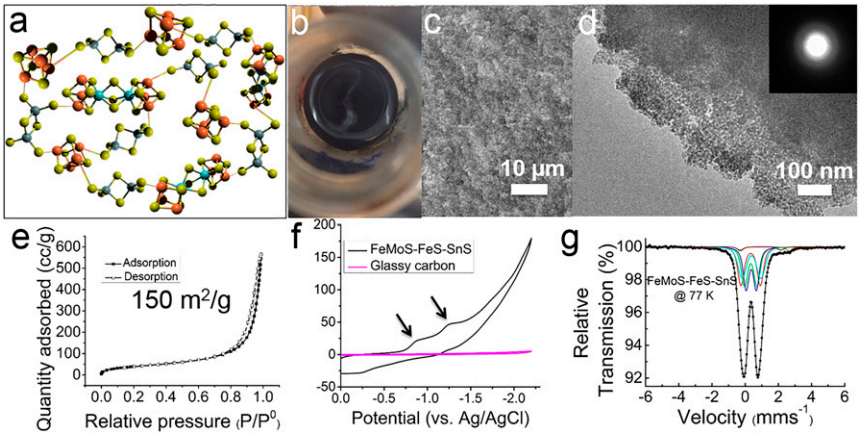

Fig. 2. Ex situ materials characterization of as-synthesized FeMoS–FeS–SnS chalcogels. (*A*) Chalcogel network consisting of "$Mo_2Fe_6S_8(SPh)_3$" and "Fe_4S_4" cores linked with $Sn_2S_6^{4-}$ clusters. (*B*) Photo of black FeMoS–FeS–SnS chalcogel. (*C* and *D*) SEM and TEM images of FeMoS–FeS–SnS chalcogel. (*D*, *Inset*) A typical chalcogel selected-area diffuse electron diffraction pattern, revealing its amorphous character. (*E*) Nitrogen adsorption/desorption isotherms obtained at 77 K from a sample of FeMoS–FeS–SnS aerogel. (*F*) CV of FeMoS–FeS–SnS chalcogel electrode at 50-mV/s scan rate. (*G*) Mössbauer spectrum of the FeMoS–FeS–SnS chalcogel recorded at 77 K.

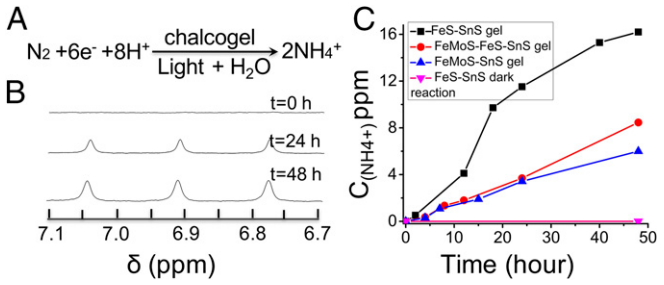

Fig. 3. Photocatalytic N_2 reduction by the chalcogels. (*A*) The standard photocatalytic reaction of N_2 reduction to NH_4^+. (*B*) Proton NMR (400 MHz) spectra showing the formation of NH_4^+ in a typical photocatalytic experiment as a function of reaction time. δ, chemical shift. (*C*) Photocatalytic N_2 reduction performance comparisons for FeMoS–SnS, FeMoS–FeS–SnS and FeS–SnS chalcogels. C(NH_4^+): concentration of NH_4^+. ppm can be expressed as milligrams per liter. One ppm equals the 1 mg of NH_4^+ in 1 L of H_2O.

materials characterizations). Compared with FeMoS–SnS chalcogel, the FeMoS–FeS–SnS chalcogel gave better yield of NH_4^+ over 48-h reaction time (30). For the FeMoS–FeS–SnS gel, the better performance can be ascribed partly to the thermodynamically favorable electron transfer from Fe_4S_4 cluster to $Mo_2Fe_6S_8(SPh)_3$ cluster under broad excitation by comparing the first reduction potential of the two clusters obtained from the CV measurements (*SI Appendix*, Figs. S4B and S5F, respectively).

Due to recent research on nitrogenase assigns iron as the N_2 binding site in the FeMoco (8), and also motivated by the higher performance of FeMoS–FeS–SnS than the FeMoS–SnS, we tested FeS–SnS for photochemical N_2 fixation (33). Remarkably, the FeS–SnS was also able to accomplish the N_2 fixation, and the NH_4^+ yield could reach as high as 16 ppm. The FeMoS–M–SnS chalcogel exhibited varied N_2 reduction activities (*SI Appendix*, Figs. S6 and S7 for materials characterizations). More specifically, the M=Sb^{3+} material boosted the performance of the pristine FeMoS–SnS chalcogel whereas the M=Sn^{4+}, Zn^{2+} chalcogels had weaker performance in terms of N_2 reduction efficiency (*SI Appendix*, Fig. S8).

A broad set of control experiments was also conducted to exclude possibilities that ammonia production might result from sources other than N_2 (*SI Appendix*, Fig. S9A). There was no ammonia detected from the ultrapure H_2O used as solvent for the reaction, excluding possible ammonia contamination from water (*SI Appendix*, Fig. S9*B*). Ammonia was not observed when the chalcogel catalyst was absent from the reaction (*SI Appendix*, Table S3, entry 3) or when the reaction was performed in the dark (with chalcogel), verifying the role of light in driving the N_2 reduction and the role of chalcogel in catalyzing it (*SI Appendix*, Table S3, entry 4 and *SI Appendix*, Fig. S9C). No ammonia was detected with $Na_4Sn_2S_6$ replacing iron–sulfur chalcogels as catalysts under standard photocatalytic N_2 reduction condition, indicating the linking agent not being involved in the photocatalytic experiment (*SI Appendix*, Fig. S9D). Turnover numbers (TON) were obtained in separate experiments over a total duration period of 96 h. An amount of 12 μmol of NH_4^+ (5.4 ppm of NH_4^+ in 40 mL of reaction solution) was obtained for 0.7 μmol of FeMoS–FeS–SnS chalcogel catalyst (TON ~ 17), indicating the catalytic nature of the N_2 reduction reaction.

The photocatalytic experiments were also run using optical filters to block the UV radiation emitted by the xenon lamp. The UV filter blocks 99% of UV light and allows ~80% of the visible light to pass through. Under these conditions, the ammonia production was retained and the yield was lowered to 50% compared with the yield without the optical filter. This demonstrates that visible light dominates the photochemical N_2 reduction reaction by FeMoS–FeS–SnS (*SI Appendix*, Table S3, entry 2).

To corroborate the origin of ammonia from N_2, we conducted an isotopic labeling study using N_2 enriched to 98% with $^{15}N{\equiv}^{14}N$ as the purge gas (Fig. 4*A*). Quantification of the obtained $^{15}NH_4^+$ was accomplished using ^1H NMR spectroscopy of the reaction solutions. The ^1H spectra show that coupling to ^{14}N is a triplet and coupling to ^{15}N is a doublet. Fig. 4*B* (*Insets*) show ^1H NMR spectra of authentic $^{14}NH_4^+$ and $^{15}NH_4^+$ in DMSO-d_6 (see 1H NMR calibration curve of authentic $^{15}NH_4Cl$ in *SI Appendix*, Fig. S10). For the isotope labeling experiment, a gas-trapping strategy was preferred due to the limited supply and high cost of $^{15}N{\equiv}^{14}N$ gas (27). The $^{15}N{\equiv}^{14}N$ gas pressure was built up in the headspace of the vial with the pressure slightly higher than that of ambient condition. (see setup for labeling experiment in *SI Appendix*, Fig. S11). The ^1H NMR results shown in Fig. 4*B* demonstrate that both triplets and doublets could be observed, which correspond to $^{14}NH_4^+$ and $^{15}NH_4^+$, respectively. The emergence of the $^{15}NH_4^+$ doublets with irradiation time provides conclusive evidence that the detected ammonia originates from nitrogen gas.

The excitation of the clusters by light illumination must form energetic enough excited states capable of binding N_2 and reducing it stepwise presumably to NH=NH, H_2N–NH_2, and ultimately NH_3. We sought to observe the binding events and possible intermediates in the early stages of this cascade using DRIFTS. The advantage of DRIFTS is the ability to analyze solids and their interaction with gases in situ and without special sample preparation. This extremely sensitive spectroscopy technique permits studies of the surface chemistry of high surface area materials, notably for heterogeneous catalysis and gas molecule binding, where in the DRIFTS cell the temperature and environment of the catalyst can be controlled in situ. The mechanism of photocatalytic conversion of N_2 over chalcogels was therefore investigated by means of in situ DRIFTS in combination with a moist stream of N_2 as well as isotopically labeled $^{15}N_2$ and D_2O (see setup in Fig. 5*A*) (34). The purpose of using moisture in this experiment was to provide a mechanism for the reaction to obtain protons. Fig. 5*B* shows DRIFTS spectra of FeMoS–FeS–SnS aerogel over 75 min of light illumination in N_2 atmosphere, against background spectra of the same gel obtained after flushing with the argon for 20 min. The

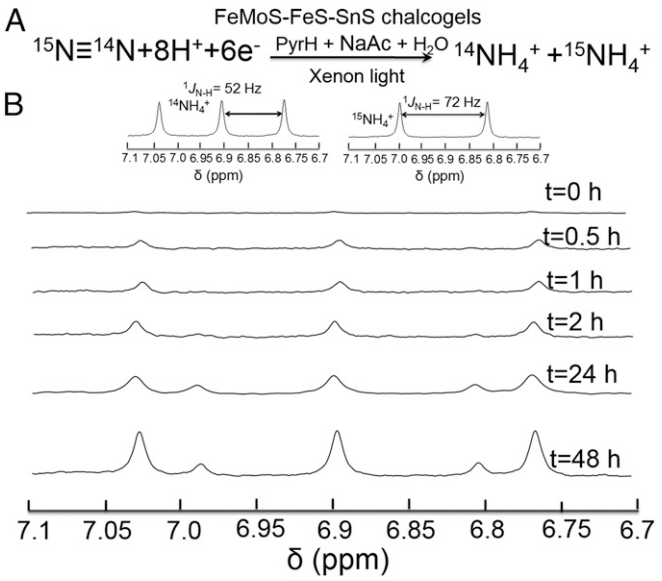

Fig. 4. Isotope labeling experiment. (*A*) Simplified equation depicting the photocatalytic isotope N_2 reduction experiment. (*B*) ^1H NMR spectra showing the formation of both $^{14}NH_4^+$ and $^{15}NH_4^+$ (corresponding to triplets and doublets, respectively) produced as a function of time from a photocatalytic run using $^{15}N{\equiv}^{14}N$ as isotopic N_2 source. (*Insets*) ^1H NMR (400 MHz) spectra of a $^{14}NH_4Cl$ sample and $^{15}NH_4Cl$ sample used as standards in DMSO-d_6, respectively.

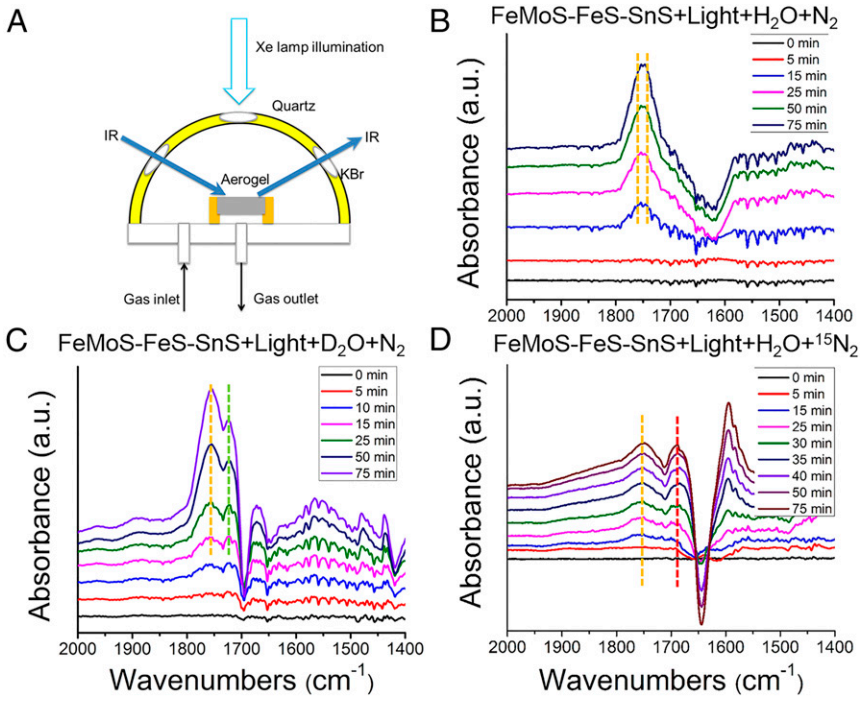

Fig. 5. In situ DRIFTS spectra from FeMoS–FeS–SnS aerogels under different conditions. (*A*) Schematic illustration of the in situ DRIFTS instrument with Xe lamp illumination. (*B*) FeMoS–FeS–SnS aerogel in the presence of flowing N_2 and H_2O. (*C*) FeMoS–FeS–SnS aerogel in the presence of flowing N_2 and D_2O with light irradiation with continuous N_2 purging. (*D*) FeMoS–FeS–SnS aerogel in the presence of flowing $^{15}N_2$ and H_2O.

spectra are dominated by two new absorption bands at 1,753 and 1,746 cm^{-1}(*SI Appendix*, Fig. S12*A*). These bands do not appear when there is no N_2 flowing or when the experiments are carried out in the dark. We attribute these two bands to the *N*–N stretching mode of an M–N=N moiety in accordance with previous studies (16, 35, 36). When D_2O was used in place of H_2O the absorption band at 1,746 cm^{-1} redshifted to 1,724 cm^{-1} while the band at 1,753 cm^{-1} band remained in place (Fig. 5*C*).The D_2O isotope experiment showed that hydrogen is only involved in the stretching mode of M–N=N species at 1,753 cm^{-1}.

The FeMoS–SnS or FeS–SnS aerogels were also investigated with DRIFTS. As shown in *SI Appendix*, Fig. S13 *A* and *B*, only one absorption band at 1,753 cm^{-1} for FeMoS–SnS and 1,746-cm^{-1} band for FeS–SnS were observed, which implies that these two absorption bands arise from the *N*–N stretching of M–N=N moiety bound on $Mo_2Fe_6S_8(SPh)_3$ and Fe_4S_4 clusters, respectively. Moreover, isotope experiments with D_2O on the isolated FeS–SnS aerogel showed a redshift of absorption band at 1,746 cm^{-1} to 1,718 cm^{-1}, similar to the observation on FeMoS–FeS–SnS aerogel (Fig. 5*C* and *SI Appendix*, Fig. S13*C*). Therefore, the absorption band at 1,753 cm^{-1} probably originates from N_2 binding to the $Mo_2Fe_6S_8(SPh)_3$ cluster (M–N=N, M:Mo or Fe), whereas the band at 1,746 cm^{-1} arises from binding to the Fe_4S_4 cluster [Fe–N=N(H)]. These frequencies match well those from a series of Fe–N_2–Fe complexes described by Holland and co-workers in the range between 1,583 and 1,810 cm^{-1} (36, 37), but are lower than that of $[Mo(N_2)_2(PNP)]_2(\mu\text{-}N_2)$ synthesized by Nishibayashi and co-workers around 1,940 cm^{-1} (10). Comparing with the stretching frequencies of the free N_2, azobenzene (PhN=NPh), and hydrazine (H_2N-NH_2) (ν_{NN} = 2,331, 1,442, and 1,111 cm^{-1}, respectively), the N≡N triple bond of N_2 weakens after binding to the chalcogel clusters, suggesting the potential for further functionalization, and ultimate *N*–N bond cleavage to form ammonia (38). The *N*–N stretching mode frequency is lower on the Fe_4S_4 cluster than on $Mo_2Fe_6S_8(SPh)_3$ cluster, implying that the photoactivated Fe_4S_4 weakens the N≡N bond more significantly (35). This could partially explain why the FeS–SnS chalcogel outperforms the FeMoS–FeS–SnS chalcogel in terms of NH_3 production.

We also conducted isotopic labeling studies with DRIFTS experiments using $^{15}N_2$. Compared with $^{14}N_2$, a new band at 1,687 cm^{-1} was observed with prolonged irradiation (Fig. 5*D*). However, a broad band (including the 1,753- and 1,746-cm^{-1} band) was also observed with an absorption band at 1,687 cm^{-1} due to the residual $^{14}N_2$ always being present in the DRIFTS cell. This isotopic band shift of ∼66 cm^{-1} from 1,753 cm^{-1} to 1,687 cm^{-1} is consistent with literature reports (19, 35–37). Our DRIFTS results demonstrate that N_2 can bind to the chalcogel under light illumination. Upon initial formation of the M–N=N intermediates, electron and proton transfer can occur followed by additional light-induced electron reduction and protonation until the N≡N bond cleavage to NH_3 in the final step (5, 39, 40). The fact that NH_2NH_2 is a far more active substrate than N_2 in yielding NH_3 explains why it is not detected as a product in our NMR spectra and suggests that NH_2NH_2 is a likely intermediate similar to the mechanism postulated for nitrogenase itself (8, 41).

To gain further insights into the binding of N_2 to the $Mo_2Fe_6S_8(SPh)_3$ and Fe_4S_4 clusters upon photoexcitation, we have used broken symmetry density functional theory (DFT) calculations using the ORCA computational chemistry package (42). We aimed to explore the potential binding between N_2 and different oxidation states of the simplified model complexes including $[Mo_2Fe_6S_8(SPh)_3Cl_6]^{3-}$ and $[Fe_4S_4Cl_4]^{2-}$. The three minus form $[Mo_2Fe_6S_8(SPh)_3Cl_6]^{3-}$ and two minus form $[Fe_4S_4Cl_4]^{2-}$, precursors of the FeMoS–FeS–SnS, FeMoS–SnS, and FeS–SnS chalcogels, respectively, were taken to be the oxidation states of the ground states of the base units of the chalcogel. These models represent only a local fraction of the chalcogels where nitrogen bonding is thought to take place; our model does not describe interactions and structural changes between units. Thus, the models are only intended to give mostly qualitative insights. The $[Mo_2Fe_6S_8(SPh)_3Cl_6]^{3-}$ has a double-cubane structure, containing four open-shell metal centers in each individual cubane: one molybdenum and three iron atoms, with the cubanes bridged by three sulfur atoms. A few high-spin solutions were selected before using the broken symmetry calculations to perform spin flips on various combinations of metal centers. The lowest energy combination for all oxidation states involved an overall antiferromagnetic coupling between the two cubanes with $M_s = 0$ for the 3^- and 5^- clusters and $M_s = 1/2$ for the 4^- cluster. The calculations for $[Fe_4S_4Cl_4]^{2-}$

proceeded in the same fashion. The lowest energy combinations involved an antiferromagnetic coupling between two groups of two iron atoms with overall $M_s = 0$ for the 2^- and 4^- clusters and $M_s = 1/2$ for the 3^- cluster.

We then simulated the electron reduction of the complex and subsequent N_2 binding and reduction by using NaAc and PyrH as electron and proton sources in accordance with the experimental conditions. For our $Mo_2Fe_6S_8(SPh)_3$ model, we found N_2 attaching to molybdenum or to a four-coordinate iron site on the doubly reduced complex as the most thermodynamically feasible mechanism after testing a number of different possible binding sites for N_2 for all oxidation states. Fig. 6 shows the adsorption energies of N_2 for different oxidation states of the clusters. As seen in Fig. 6*A*, attempting to bind N_2 to Mo incurs a penalty of about 10 kcal/mol when the cluster is unreduced. After reducing the cluster twice to its 5^- state ($[Mo_2Fe_6S_8(SPh)_3Cl_6]^{5-}$), the same binding becomes favorable by about 7 kcal/mol. Almost the same thermodynamics are observed in Fig. 6*B* when N_2 binds to Fe in the $Mo_2Fe_6S_8(SPh)_3$ model cluster. In the ground state, the energy penalty is about 30 kcal/mol, but, after the complex is reduced twice to the 5^- state, N_2 binding becomes favorable by about 8 kcal/mol. For both cases in Fig. 6 *A* and *B*, reducing the complex only once to the 4^- state leads to N_2 adsorption energies that are slightly favorable or thermodynamically neutral. For $[Fe_4S_4Cl_4]^{2-}$, the same trends in behavior with reducing the complex occur as seen in Fig. 6*C*. However, N_2 binding is very unfavorable in both the unreduced and singly reduced 2^- and 3^- states by about 30 and 20 kcal/mol, respectively. The doubly reduced 4^- state still exhibits much less unfavorable N_2 binding, by about 5 kcal/mol, suggesting that such binding might be feasible. Because of the complexity of the calculations, transition state barriers were not included. Future work in this area could test whether N_2 prefers to bind to Mo or Fe in the $Mo_2Fe_6S_8(SPh)_3$ clusters because their binding energies are so similar. The calculated potential energy levels of Fig. 6 indicate that reduction of the chalcogel, here hypothesized as photoinduced, is required to obtain thermodynamically favorable or nearly thermodynamically favorable N_2 adsorption energies.

For all tested oxidation states of $Mo_2Fe_6S_8(SPh)_3$ clusters, forming a species linking N_2 and Mo requires sulfur bridging ligands to leave the Mo atom and move over to the opposite Mo atom, as seen in Fig. 6*A*. Forming a similar species with N_2 and Fe linked (Fig. 6*B*) requires removal of the chloride ligand from the Fe to form a roughly tetrahedral structure with the iron atom, which would correspond to breaking one of the Fe–S–Sn bridges in the full chalcogel. Localized orbital analysis shows no bonding orbitals or extremely weak bonding orbitals between N_2 and metal atoms for all tested oxidation states, suggesting an interaction dominated by van der Waals forces. In the case of $[Fe_4S_4Cl_4]^{2-}$ (Fig. 6*C*), the N_2 binding is similar to N_2 binding to iron in the double $Mo_2Fe_6S_8(SPh)_3$ cubane; a chloride ligand is removed, and localized orbital analysis shows a very weak bonding orbital between nitrogen and iron.

Whereas the nitrogen–metal interaction in Fig. 6 *A* and *B* is more favorable for the reduced form of the $Mo_2Fe_6S_8(SPh)_3$ model, this interaction does not necessarily suggest that $Mo_2Fe_6S_8(SPh)_3$ has faster kinetics and a higher yield than the Fe_4S_4 cluster. These energetics merely demonstrate when nitrogen binding is most feasible. A better indicator of theoretical agreement with the DRIFTS experiments can be found in the calculated *N*–N bond lengths indicated in Fig. 6. For the $Mo_2Fe_6S_8(SPh)_3$ cluster, the calculated *N*–N bond lengths are 1.099 Å and 1.111 Å when nitrogen attaches to Mo and Fe in the 5^- state, respectively. These distances lie in between bond length values of free nitrogen (1.098 Å) and diazine (1.201 Å). In the Fe_4S_4 cluster, the calculated N≡N bond length is 1.116 Å, which is about 0.02 Å longer than the reported bond length of free nitrogen. This result suggests that the interaction between nitrogen and transition metal weakens the N≡N bond most in the case of the Fe_4S_4 cluster, in agreement with the DRIFTS experiment.

In summary, redox-active bioinspired iron-containing sulfide clusters can form high-energy photoexcited states that bind and convert N_2 to NH_3. The presence of Fe in the chalcogels seems to be necessary for this process whereas that of Mo is not. Specifically, whereas $Mo_2Fe_6S_8(SPh)_3$ with Fe_4S_4 clusters coexisting in a single chalcogel structure can boost NH_3 production over $Mo_2Fe_6S_8(SPh)_3$ alone, the Fe_4S_4-only chalcogel (FeS–SnS) is not only also active in photochemical N_2 reduction but exhibits higher ammonia yield. Although this result suggests that Fe is the active site for N_2 binding, it does not preclude Mo playing a role in N_2 binding. Mechanistically, the N_2 binding on the metal site [Mo or Fe for $Mo_2Fe_6S_8(SPh)_3$; Fe for Fe_4S_4] occurs upon multiple reduction (achieved with multiphoton excitation) of the clusters and the intermediate M–N=N moiety is observable by DRIFTS via the bands at 1,753 or 1,746 cm^{-1}, respectively. DFT calculations suggest that the formation of M–N=N intermediate from N_2 binding to multiply reduced $Mo_2Fe_6S_8(SPh)_3$ and Fe_4S_4 clusters is feasible, which can then activate N_2 toward final ammonia formation. The results reported here will greatly expand the scope of materials design and engineering for the creation of highly active N_2 reduction catalysts operating in ambient conditions.

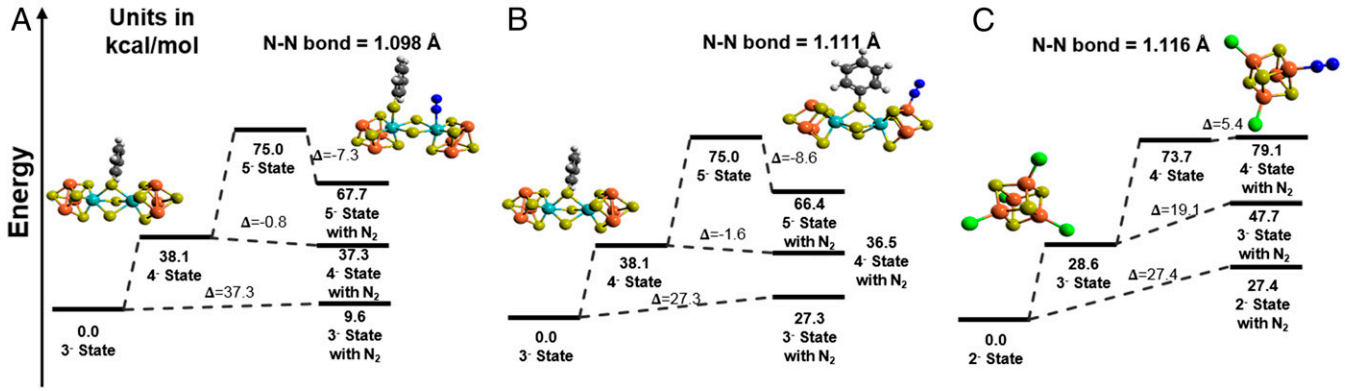

Fig. 6. Potential energy levels of $Mo_2Fe_6S_8(SPh)_3$ and Fe_4S_4 models catalyzed nitrogen-fixation reaction. Calculated potential energy level in kcal/mol for N_2 adsorption energies to clusters. Mo = blue, Fe = orange, S = yellow, C= gray, and H = white. Two phenyl groups and Cl atoms have been removed for a clear view of the active site. For all cases, the complexes start in their unreduced ground state (3^- for $[Mo_2Fe_6S_8(SPh)_3Cl_6]^{3-}$ and 2^- for $[Fe_4S_4Cl_4]^{2-}$). From there, they can be reduced once or twice, to $[Mo_2Fe_6S_8(SPh)_3Cl_6]^{4-}$ and $[Mo_2Fe_6S_8(SPh)_3Cl_6]^{5-}$ (denoted 4^- and 5^- states for the $Mo_2Fe_6S_8$ clusters) or to $[Fe_4S_4Cl_4]^{3-}$ and $[Fe_4S_4Cl_4]^{4-}$ (denoted 3^- and 4^- states for the Fe_4S_4 clusters). At each oxidation state, they may adsorb N_2. The potential energy level for N_2 binding with Mo (*A*) or Fe (*B*) on the $Mo_2Fe_6S_8(SPh)_3$ cluster. (*C*) The thermodynamic behavior when N_2 binds with Fe on the Fe_4S_4 cluster.

Materials and Methods

Additional details regarding the materials and methods may be found in the *SI Appendix*.

Preparation of FeMoS–FeS–SnS chalcogel. FeMoS–FeS–SnS chalcogel was prepared by mixing $(NBu_4)_3[Mo_2Fe_6S_8(SPh)_3Cl_6]$, $(Ph_4P)_2[Fe_4S_4Cl_4]$, and $Na_4Sn_2S_6{\cdot}14H_2O$ linker. To obtain a gel: (*i*) First, 0.12 mmol of $Na_4Sn_2S_6{\cdot}14H_2O$ was dissolved in 1 mL of *N*-methylformamide in a vial. (*ii*) In a separate vial, 0.12 mmol of $Mo_2Fe_6S_8(SPh)_3$ and Fe_4S_4 (in equal ratio) was dissolved in 1 mL of N, *N*-dimethylformamide, respectively. (*iii*) This solution was then slowly added to the $Na_4Sn_2S_6{\cdot}14H_2O$ solution. The $Na_4Sn_2S_6{\cdot}14H_2O$ solution is shaken manually during addition. When the addition is complete, a viscous black liquid results. This liquid is left undisturbed at room temperature for 1 wk. At that time, the viscous liquid has completely solidified into a black gel. (*iv*) The gel is subjected to cleaning by solvent exchange with ethanol and H_2O. After cleaning, the chalcogel is ready for photocatalytic use or for further characterizations.

Photocatalytic N_2 Fixation Experiment. The reaction vial contains 55 mg (50 mM) pyridinium hydrochloride and 10 mg (5 mM) sodium ascorbate in 10 mL water and was sealed with a rubber septum. Chalcogels was suspended in the aqueous solution during stirring. Nitrogen gas was continually bubbled through the solution. The solutions were continuously irradiated with a 150-W xenon lamp. The light intensity at the sample was set to 100 mW/cm^2. For all of the following experiments herein, the constant amount of wet chalcogels (150 mg) was used for comparison purpose. The N_2 flow was maintained during illumination period and flow velocity was minimized to reduce evaporation of aqueous solution in total 48-h illumination period. Quantitative proton NMR was used to quantitate ammonium concentration by using 1 mM Maleic acid as internal standard. For the NMR studies, the pH of the solutions was adjusted to 2 using concentrated hydrochloric acid aqueous solution. The 1 mM Maleic acid was used as the internal standard; 20% DMSO-d_6 was used in the solutions. NMR measurements were done on an Agilent 400-MHz system. The integration areas of triplet peaks could be used to determine the concentration of generated NH_4^+ comparing with the as-known Maleic acid reference (see the calibration curve of authentic NH_4Cl in *SI Appendix*, Fig. S3*A*).

N_2 Isotope Labeling Experiments. Labeled $^{15}N{\equiv}^{14}N$ gas was used to confirm that the obtained ammonia originates form N_2 and not some other nitrogenous sources. The $^{15}N{\equiv}^{14}N$ gas was purchased from Sigma-Aldrich Chemical Company and received without any change. For ^{15}N isotope labeling experiments, a gas-trapping system was adopted due to limited supply and expensive cost of $^{15}N{\equiv}^{14}N$. The $^{15}N{\equiv}^{14}N$ gas pressure was built up in the headspace of the vial with pressure slightly higher than that of ambient condition to contain enough $^{15}N{\equiv}^{14}N$ source. Light from a xenon lamp was illuminated onto the vial. Regularly, a certain amount of aliquot (0.5 mL) was extracted from the vial. Quantification of obtained $^{15}NH_3$ was accomplished directly by using ^1H-^{15}N NMR studies.

DRIFTS Spectra. In situ DRIFTS spectra were acquired using a Nicolet 6700 infrared spectrometer equipped with a liquid nitrogen cooled MCT-B (mercury cadmium telluride) detector. All spectra were acquired by averaging 32 scans at 4-cm^{-1} resolution, and were referenced to a certain background, which was a spectrum of the samples after they were purged with argon for at least 30 min. A typical experiment was conducted under the following conditions consecutively: (*i*) purge the cell with argon completely to remove any possible volatile contamination in the dark; (*ii*) preadsorb trace amount of water into aerogel sample surface by humidified argon in the dark; (*iii*) purge the cell with argon again to remove the surplus water in the dark; (*iv*) purge the cell with N2 in the dark; (*v*) turn on the lamp while purging the cell continually with N_2.

ACKNOWLEDGMENTS. We acknowledge the Integrated Molecular Structure Education and Research Center facility at Northwestern University for NMR investigation and Electron Probe Instrumentation Center at Northwestern University for electron microscopy and elemental analysis. This work was supported as part of the ANSER Center, an Energy Frontier Research Center funded by the US Department of Energy, Office of Science, Office of Basic Energy Sciences, under Award DE-SC0001059.

1. Smil V (2004) *Enriching the Earth: Fritz Haber, Carl Bosch, and the Transformation of World Food Production* (MIT Press, Cambridge, MA).
2. Hoffman BM, Lukoyanov D, Yang Z-Y, Dean DR, Seefeldt LC (2014) Mechanism of nitrogen fixation by nitrogenase: The next stage. *Chem Rev* 114(8):4041–4062.
3. Howard JB, Rees DC (2006) How many metals does it take to fix N_2? A mechanistic overview of biological nitrogen fixation. *Proc Natl Acad Sci USA* 103(46):17088–17093.
4. Beinert H, Holm RH, Münck E (1997) Iron-sulfur clusters: Nature's modular, multipurpose structures. *Science* 277(5326):653–659.
5. Anderson JS, Rittle J, Peters JC (2013) Catalytic conversion of nitrogen to ammonia by an iron model complex. *Nature* 501(7465):84–87.
6. Owens CP, Katz FE, Carter CH, Luca MA, Tezcan FA (2015) Evidence for functionally relevant encounter complexes in nitrogenase catalysis. *J Am Chem Soc* 137(39):12704–12712.
7. Shilov A, et al. (1971) New nitrogenase model for reduction of molecular nitrogen in protonic media. *Nature* 231(5303):460–461.
8. Hoffman BM, Dean DR, Seefeldt LC (2009) Climbing nitrogenase: Toward a mechanism of enzymatic nitrogen fixation. *Acc Chem Res* 42(5):609–619.
9. Lancaster KM, et al. (2011) X-ray emission spectroscopy evidences a central carbon in the nitrogenase iron-molybdenum cofactor. *Science* 334(6058):974–977.
10. Arashiba K, Miyake Y, Nishibayashi Y (2011) A molybdenum complex bearing PNP-type pincer ligands leads to the catalytic reduction of dinitrogen into ammonia. *Nat Chem* 3(2):120–125.
11. Yandulov DV, Schrock RR (2003) Catalytic reduction of dinitrogen to ammonia at a single molybdenum center. *Science* 301(5629):76–78.
12. Miyazaki T, et al. (2014) Cleavage and formation of molecular dinitrogen in a single system assisted by molybdenum complexes bearing ferrocenyldiphosphine. *Angew Chem Int Ed Engl* 53(43):11488–11492.
13. Macleod KC, Holland PL (2013) Recent developments in the homogeneous reduction of dinitrogen by molybdenum and iron. *Nat Chem* 5(7):559–565.
14. Kuriyama S, et al. (2014) Catalytic formation of ammonia from molecular dinitrogen by use of dinitrogen-bridged dimolybdenum-dinitrogen complexes bearing PNP-pincer ligands: Remarkable effect of substituent at PNP-pincer ligand. *J Am Chem Soc* 136(27):9719–9731.
15. Li Y, et al. (2013) Ammonia formation by a thiolate-bridged diiron amide complex as a nitrogenase mimic. *Nat Chem* 5(4):320–326.
16. Kuriyama S, et al. (2015) Nitrogen fixation catalyzed by ferrocene-substituted dinitrogen-bridged dimolybdenum–dinitrogen complexes: Unique behavior of ferrocene moiety as redox active site. *Chem Sci (Camb)* 6(7):3940–3951.
17. Shima T, et al. (2013) Dinitrogen cleavage and hydrogenation by a trinuclear titanium polyhydride complex. *Science* 340(6140):1549–1552.
18. Nishibayashi Y (2015) Recent progress in transition-metal-catalyzed reduction of molecular dinitrogen under ambient reaction conditions. *Inorg Chem* 54(19):9234–9247.
19. Čorić I, Mercado BQ, Bill E, Vinyard DJ, Holland PL (2015) Binding of dinitrogen to an iron-sulfur-carbon site. *Nature* 526(7571):96–99.
20. Zhu D, Zhang L, Ruther RE, Hamers RJ (2013) Photo-illuminated diamond as a solid-state source of solvated electrons in water for nitrogen reduction. *Nat Mater* 12(9):836–841.
21. Christianson JR, Zhu D, Hamers RJ, Schmidt JR (2014) Mechanism of N_2 reduction to NH3 by aqueous solvated electrons. *J Phys Chem B* 118(1):195–203.
22. Rusina O, Eremenko A, Frank G, Strunk HP, Kisch H (2001) Nitrogen photofixation at nanostructured iron titanate films. *Angew Chem Int Ed Engl* 40(21):3993–3995.
23. Oshikiri T, Ueno K, Misawa H (2014) Plasmon-induced ammonia synthesis through nitrogen photofixation with visible light irradiation. *Angew Chem Int Ed Engl* 53(37):9802–9805.
24. Li H, Shang J, Ai Z, Zhang L (2015) Efficient visible light nitrogen fixation with BiOBr nanosheets of oxygen vacancies on the exposed 001 facets. *J Am Chem Soc* 137(19):6393–6399.
25. Bag S, Trikalitis PN, Chupas PJ, Armatas GS, Kanatzidis MG (2007) Porous semiconducting gels and aerogels from chalcogenide clusters. *Science* 317(5837):490–493.
26. Bag S, Gaudette AF, Bussell ME, Kanatzidis MG (2009) Spongy chalcogels of non-platinum metals act as effective hydrodesulfurization catalysts. *Nat Chem* 1(3):217–224.
27. Yuhas BD, et al. (2011) Biomimetic multifunctional porous chalcogels as solar fuel catalysts. *J Am Chem Soc* 133(19):7252–7255.
28. Yuhas BD, Prasittichai C, Hupp JT, Kanatzidis MG (2011) Enhanced electrocatalytic reduction of CO_2 with ternary Ni-Fe_4S_4 and Co-Fe_4S_4-based biomimetic chalcogels. *J Am Chem Soc* 133(40):15854–15857.
29. Yuhas BD, Smeigh AL, Douvalis AP, Wasielewski MR, Kanatzidis MG (2012) Photocatalytic hydrogen evolution from FeMoS-based biomimetic chalcogels. *J Am Chem Soc* 134(25):10353–10356.
30. Banerjee A, et al. (2015) Photochemical nitrogen conversion to ammonia in ambient conditions with FeMoS-chalcogels. *J Am Chem Soc* 137(5):2030–2034.
31. Shim Y, et al. (2013) Tunable biomimetic chalcogels with Fe_4S_4 cores and $[Sn_{(n)}S_{(2n+2)}]^{(4-)}$ (n = 1, 2, 4) building blocks for solar fuel catalysis. *J Am Chem Soc* 135(6):2330–2337.
32. Shim Y, et al. (2014) Enhanced photochemical hydrogen evolution from Fe_4S_4-based biomimetic chalcogels containing M^{2+} (M = Pt, Zn, Co, Ni, Sn) centers. *J Am Chem Soc* 136(38):13371–13380.
33. Tran CT, Kim E (2012) Acid-dependent degradation of a [2Fe-2S] cluster by nitric oxide. *Inorg Chem* 51(19):10086–10088.
34. Yang C-C, Yu Y-H, van der Linden B, Wu JC, Mul G (2010) Artificial photosynthesis over crystalline TiO_2-based catalysts: Fact or fiction? *J Am Chem Soc* 132(24):8398–8406.
35. Ding K, et al. (2009) Cobalt-dinitrogen complexes with weakened N-N bonds. *J Am Chem Soc* 131(27):9471–9472.
36. Smith JM, et al. (2006) Studies of low-coordinate iron dinitrogen complexes. *J Am Chem Soc* 128(3):756–769.
37. Smith JM, et al. (2001) Stepwise reduction of dinitrogen bond order by a low-coordinate iron complex. *J Am Chem Soc* 123(37):9222–9223.
38. MacKay BA, Fryzuk MD (2004) Dinitrogen coordination chemistry: On the biomimetic borderlands. *Chem Rev* 104(2):385–401.
39. Chatt J, Dilworth JR, Richards RL (1978) Recent advances in the chemistry of nitrogen fixation. *Chem Rev* 78(6):589–625.
40. Seefeldt LC, Hoffman BM, Dean DR (2009) Mechanism of Mo-dependent nitrogenase. *Annu Rev Biochem* 78:701–722.
41. Demadis KD, Coucouvanis D (1995) Synthesis, structural characterization, and electronic structures of the mixed terminal ligand iron-sulfur cubanes $[Fe_4S_4Cl_2(XPh)_2]^{2-}$ (X=S, O) and $[Fe_4S_4(SPh)_2(OC_6H_4\text{-}p\text{-}CH_3)_2]^{2-}$. The first examples of $[Fe_4S_4]^{2+}$ cores with a noncompressed D_{2d} idealized geometry. *Inorg Chem* 34(14):3658–3666.
42. Neese F (2012) The ORCA program system. *Wiley Interdiscip Rev Comput Mol Sci* 2(1):73–78.